AGU PUBLICATIONS

JGR

Journal of Geophysical Research: Oceans

RESEARCH ARTICLE

10.1002/2014JC010188

Key Points:
- Proteinaceous compounds represent a large fraction of gels in marine microlayer
- Microbial activity mediates organic composition of the sea-surface microlayer
- Ocean acidification can affect the organic composition of the microlayer

Supporting Information:
- Readme
- Graphical abstract/diagram

Correspondence to:
A. Engel,
aengel@geomar.de

Citation:
Galgani, L., C. Stolle, S. Endres, K. G. Schulz, and A. Engel (2014), Effects of ocean acidification on the biogenic composition of the sea-surface microlayer: Results from a mesocosm study, *J. Geophys. Res. Oceans*, *119*, doi:10.1002/2014JC010188.

Received 26 MAY 2014
Accepted 17 OCT 2014
Accepted article online 24 OCT 2014

Effects of ocean acidification on the biogenic composition of the sea-surface microlayer: Results from a mesocosm study

Luisa Galgani[1,2], Christian Stolle[3], Sonja Endres[1], Kai G. Schulz[1,4], and Anja Engel[1]

[1]Geomar Helmholtz Centre for Ocean Research, Kiel, Germany, [2]Alfred Wegener Institute, Helmholtz Centre for Polar and Marine Research, Bremerhaven, Germany, [3]Leibniz Institute for Baltic Sea Research, Rostock, Germany, [4]School of Environmental Science and Management, Centre for Coastal Biogeochemistry, Southern Cross University, Lismore, New South Wales, Australia

Abstract The sea-surface microlayer (SML) is the ocean's uppermost boundary to the atmosphere and in control of climate relevant processes like gas exchange and emission of marine primary organic aerosols (POA). The SML represents a complex surface film including organic components like polysaccharides, proteins, and marine gel particles, and harbors diverse microbial communities. Despite the potential relevance of the SML in ocean-atmosphere interactions, still little is known about its structural characteristics and sensitivity to a changing environment such as increased oceanic uptake of anthropogenic CO_2. Here we report results of a large-scale mesocosm study, indicating that ocean acidification can affect the abundance and activity of microorganisms during phytoplankton blooms, resulting in changes in composition and dynamics of organic matter in the SML. Our results reveal a potential coupling between anthropogenic CO_2 emissions and the biogenic properties of the SML, pointing to a hitherto disregarded feedback process between ocean and atmosphere under climate change.

1. Introduction

Recent studies have emphasized that the composition of the SML is characterized by high abundance of marine gel particles [*Cunliffe and Murrell*, 2009; *Wurl and Holmes*, 2008], hydrated organic supramolecular structures vitally important for microbial processes and carbon cycling in the ocean [*Passow*, 2002b]. Hydrogels originate from high molecular weight polymers like polysaccharides and peptides that are released by phytoplankton and bacterioplankton cells during growth and decay [*Chin et al*., 1998; *Engel et al*., 2004]. In an initial step, these polymers assemble to water insoluble colloidal nano and microgels [*Chin et al*., 1998; *Verdugo et al*., 2004], and further aggregate to larger particles of several millimeters size [*Engel et al*., 2004; *Verdugo*, 2012]. Polysaccharidic gels in the ocean, such as transparent exopolymer particles (TEP), have been attributed mainly to phytoplankton exudation [*Passow*, 2002b], while the production of protein-containing gels, such as coomassie stainable particles (CSP) has been related to cell lysis and decomposition, as well as to the absorption of proteins onto nonproteinaceous particles [*Long and Azam*, 1996]. Physical accumulation of gels particles in the SML can result from gels ascending the water column due to their low density, and by adsorption of gels or gel precursors onto rising bubbles [*Azetsu and Passow*, 2004; *Zhou et al*., 1998].

Polysaccharidic and proteinaceous gels may be closely associated, but are operationally confined into two distinct classes according to analytical techniques [*Engel*, 2009]. In the ocean, and also within the SML, organic gel particles represent substrates for marine phytoplankton and bacterioplankton to attach and grow upon, facilitating the formation of an active biofilm [*Cunliffe et al*., 2011; *Flemming and Wingender*, 2010; *Long and Azam*, 1996; *Passow*, 2002b]. In addition to gels ascending from the water column, de novo production of gels can occur within the SML due to compression of dissolved organic matter (DOM) during surface wave action [*Wurl et al*., 2011b], or as a consequence of photochemical and bacterial breakdown of particles [*Lechtenfeld et al*., 2013]. Waves and turbulent shear may further facilitate the collision and aggregation of gels within the SML [*Kuznetsova et al*., 2005; *Wurl and Holmes*, 2008].

Organic particles in the SML, such as marine gels, might provide a new source for submicron POA during the emission of sea spray to the lower atmosphere [*Leck and Bigg*, 2005]. Water insoluble organic particles dominate total submicron marine aerosol mass during bloom periods [*O'Dowd et al*., 2004]. These particles

originating by bubble bursting events have a polysaccharidic composition [*Russell et al*., 2010] and are suggested to act as cloud condensation nuclei (CCN) in regions such as the high Arctic, where low-level clouds play a climate-regulating role by reflecting incoming solar radiation [*Leck and Bigg*, 2005; *Orellana et al*., 2011]. Moreover, it has been suggested that amino acids and proteinaceous gels become enriched in SML and sea-spray aerosols [*Kuznetsova et al*., 2005]. Marine POA-cloud feedback processes are an emerging issue in present day and future scenarios of surface ocean-lower atmosphere interactions, due to their high potential of controlling earth's radiation budget and energy fluxes [*Solomon et al*., 2007]. Despite their suggested role as marine source for POA [*Quinn and Bates*, 2011], still little is known about the factors controlling the accumulation, size distribution, and composition of gels in the SML.

The ocean is known to act as a net sink for atmospheric carbon dioxide (CO_2) [*Sabine et al*., 2004]. Therefore, the continuous increase in atmospheric anthropogenic CO_2 concentration leads to a progressive decline in ocean's pH [*Caldeira and Wickett*, 2003; *Sabine et al*., 2004]. This is known as ocean acidification [*Caldeira and Wickett*, 2003], with potential consequences for marine microbial activity [*Endres et al*., 2014; *Engel et al*., 2013; *Grossart et al*., 2006; *Piontek et al*., 2010]. In the ocean, rising uptake of anthropogenic CO_2 may enhance autotrophic carbon fixation and increase the extracellular release of organic polymers from phytoplankton [*Engel et al*., 2013; *Hein and Sand-Jensen*, 1997]. Thereby, a high production of extracellular polymers supports the accumulation of gel particles [*Borchard and Engel*, 2012; *Engel*, 2002] that may contribute to surface biofilm formation. Enhanced organic matter production might be counteracted by higher heterotrophic activity under future ocean conditions [*Piontek et al*., 2010], and thus changing the balance of autotrophy versus heterotrophy with possible positive feedbacks on rising atmospheric CO_2 [*Del Giorgio and Duarte*, 2002].

Here we show results from a large-scale pH perturbation experiment with the Kiel Off-Shore Mesocosms for future Ocean Simulation (KOSMOS) in Raunefjord, Norway, in the aftermath of a spring bloom. The aim of this study was to examine the coupling between phytoplankton bloom development and the accumulation, composition and microbial dynamics of organic matter in the SML in response to CO_2 enrichment as expected for future ocean acidification scenarios.

2. Methods

2.1. Experimental Setup

Between 8 May 2011 and 6 June 2011, we sampled six KOSMOS mesocosms with a water volume of $\sim$75 m^3. Two mesocosms with a field pCO_2 of about 300 μatm were used as control and left without CO_2 addition (mesocosms 2 and 4), while four mesocosms were adjusted to initial target pCO_2 levels of 600 (mesocosm 8), 900 (mesocosm 1), 1300 (mesocosm 5), and 2000 μatm (mesocosm 7) obtained by the progressive addition of CO_2-rich seawater as described in *Riebesell et al*. [2013] and *Endres et al*. [2014]. The CO_2 addition was finalized on experimental day 5. In the afternoon of experimental day 14 (22 May), nutrients were added to all mesocosms to a final concentration of 5 μmol L^{-1} nitrate and 0.16 μmol L^{-1} phosphate in order to stimulate a phytoplankton bloom. Median pH values of the whole period at in situ temperature ranged from 8.10 in control (mesocosms 2 and 4) to 7.56 at the highest pCO_2 level (mesocosm 7). Water temperature ranged from 6.8°C at the beginning of the experiment to 10.0°C at the end.

SML sampling started 1 day before the first CO_2 addition (termed "day −1") and was repeated every second day between 7 and 9 am, before the main sampling of the mesocosms water column. Previous studies, including mesocosms experiments, have investigated the time of SML reformation and consistently show that chemical and biological components as well as microbial activity within the SML reestablish quickly after a disruption with observed timescales being typically <1 min [see *Cunliffe et al*., 2013, for review].

SML samples were collected with a glass plate sampler [*Harvey and Burzell*, 1972], made of silicate glass (5 mm thickness) and with an effective surface area of 5600 cm^2 (considering both sides). For each sample, the glass plate was inserted into the water perpendicular to the surface and withdrawn at a controlled rate of $\sim$20 cm s^{-1}. The sample, retained on the glass because of surface tension, was removed with the help of a Teflon wiper. For each sample, the procedure was repeated three times. Samples were collected into acid cleaned (HCl, 10%) and Milli-Q washed glass bottles. Prior to sampling, both glass plate and wiper were washed with HCl (10%) and intensively rinsed with Milli-Q water. Between samplings, both instruments were copiously rinsed with fjord water in order to minimize their contamination with alien material while

handling or transporting the devices. The surface area of each mesocosms was about 31,416 cm^2, and allowed only for a limited sampling. Therefore, SML samples from similar pCO_2 levels were combined for analyses: mesocosms 2 and 4, as control, mesocosms 1 and 8, as medium pCO_2, and mesocosms 5 and 7 as high pCO_2.

The SML thickness (d, cm) was estimated as follows:

$$d = V/A \quad (1)$$

where V is the SML volume collected, i.e., 60–140 mL, and A is 3 times the sampling area of the glass plate (A = 16,800 cm^2). Assuming a maximum thickness of the SML of 100 $\times$ 10^{-4} cm, and considering the sampling area of the mesocosms, we choose to standardize our sampling procedure to three dips of the glass plate to avoid dilution with the underlying water. During this study, d ranged from 36 to 89 $\times$ 10^{-4} cm, increasing during the development of the phytoplankton blooms. Throughout the whole experiment, the SML thickness was not significantly different between mesocosms (Kruskal-Wallis one way ANOVA on ranks, $p = 0.442$). Average values for d were in fact very similar: for the control treatment $d = 61 \pm 11 \times 10^{-4}$ cm (mesocosm 2) and 64 $\pm$ 11 $\times$ 10^{-4} cm (mesocosm 4), for medium pCO_2 treatment $d = 68 \pm 11 \times 10^{-4}$ cm (mesocosm 8) and 63 $\pm$ 9 $\times$ 10^{-4} cm (mesocosm 1), for high pCO_2 treatment $d = 64 \pm 12 \times 10^{-4}$ cm (mesocosm 5) and 64 $\pm$ 9 $\times$ 10^{-4} cm (mesocosm 7).

2.2. Parameters and Statistical Analysis

Chlorophyll a (μg L^{-1}) from the mesocosms water column (depth-integrated between 0.3 and 23 m) was determined with a TURNER 10-AU fluorometer according to *Welschmeyer* [1994]. Samples were prepared by filtering 250–500 mL onto GF/F filters (Whatmann), stored at −80°C for at least 24 h, and homogenized in 90% acetone using glass beads (2 and 4 mm) in a cell mill. Results are shown as averages of mesocosms 2 and 4 (control), mesocosms 1 and 8 (medium pCO_2), and mesocosms 5 and 7 (high pCO_2). For a detailed description of chlorophyll a in the water column of individual mesocosms, we refer to *Endres et al*. [2014].

For total hydrolysable amino acids (THAA), 5 mL of sample was filled into precombusted glass vials (8 h, 500°C) and stored at −20°C until analysis. Analysis was performed according to *Lindroth and Mopper* [1979]. Duplicate samples were analyzed with a detection limit of 2 nM on a HPLC system (1260, Agilent). Thirteen different amino acids were separated with a C18 column (Phenomenex Kinetex, 2.6 μm, 150 × 4.6 mm) after in-line derivatization with o-phtaldialdehyde and mercaptoethanol. For total combined carbohydrates >1 kDa (TCCHO), 15 mL was filled into precombusted glass vials (8 h, 500°C) and kept frozen at −20°C until analysis. The analysis was conducted according to *Engel and Händel* [2011] applying HPAEC-PAD on a Dionex ICS 3000. Samples were desalinated by membrane dialysis (1 kDa MWCO, Spectra Por) for 5 h at 6°C, hydrolyzed for 20 h at 100°C with 0.8 M HCl final concentration, and neutralized through acid evaporation (N_2, 5 h, 50°C) Two replicate samples were analyzed. For bacterial cell numbers, 1 mL sample was fixed with 100 μL paraformaldehyde (1% final concentration)/glutaraldehyde (0.05% final concentration) for 30 min in the dark, and stored at −80°C until enumeration. Samples were stained with SYBR Green I (Molecular Probes). Heterotrophic bacteria were enumerated using a flow cytometer (Becton & Dickinson FACScalibur) equipped with a laser emitting at 488 nm and detected by their signature in a plot of side scatter (SSC) versus green fluorescence (FL1). Yellow-green latex beads (Polysciences, 0.5 μm) were used as internal standard. Based on the bacterial abundances, bacterial nitrogen (N_{bac}) and carbon (C_{bac}) concentrations were calculated, assuming 2.2 $\pm$ 0.3 fg $cell^{-1}$ N and 9 $\pm$ 1 fg $cell^{-1}$ C for bacteria in Raunefjord in June [*Fagerbakke et al*., 1996].

Phytoneuston, i.e., phytoplankton cells collected from the SML, were also determined by flow cytometry following the protocol of *Marie et al*. [2010] and using 1 mL samples. Phytoneuston cells were fixed, and stored as bacteria cells. Cell abundance and size clusters were detected without staining by their signature in a plot of orange versus red fluorescence. Latex beads (3 μm) were used as internal standard.

Incorporation of ^{3}H-methyl-thymidine (^{3}H-TdR, 60.1 Ci $mmol^{-1}$, 50 nM final concentration, Hartmann Analytics) and ^{14}C-leucine (261 mCi $mmol^{-1}$, 50 nM final concentration, Hartmann Analytics) was measured to estimate bacterial biomass production (BP) in 2.5 mL water samples according to the method of *Chin-Leo and Kirchman* [1988]. Duplicate samples were incubated for 60–90 min at the in situ temperature in the dark. Incorporation was stopped by addition of formaldehyde (10% v/w) and fixation in the dark at 5°C. A third sample, serving as a blank, was fixed for at least 10 min prior to the addition of substrates. Samples

were filtered first onto 3 μm polycarbonate filters (Millipore) to determine BP of particle-associated bacteria. The filtrate was subsequently filtered onto 0.2 μm polycarbonate filters (Millipore) to determine BP of the fraction <3 μm. Activity of samples was measured in a scintillation counter (Packard) after addition of 4 mL scintillation cocktail. Particle-associated activity was below the detection limit for nearly all samples, indicating very low contribution of the size-fraction >3 μm to total BP. Thus, only BP of the fraction <3 μm is presented here. In order to allow for direct comparison with the chemical data, results of microbial abundance and BP were combined as follows: control (mesocosms 2 and 4), medium pCO_2 (mesocosms 1 and 8), and high pCO_2 (mesocosms 5 and 7).

Total area, particle numbers, and equivalent spherical diameter (d_p) of gel particles were determined by microscopy after *Engel* [2009]. Therefore, 20–30 mL were filtered onto 0.4 μm Nuclepore membranes (Whatmann) and stained with 1 mL Alcian Blue solution for polysaccharidic gels and 1 mL Coomassie Brilliant Blue G (CBBG) working solution for proteinaceous gels. Filters were mounted onto Cytoclear© slides and stored at −20°C until microscopy analysis.

The size-frequency distribution of polysaccharidic and proteinaceous gels was described by:

$$dN/d(d_p) = kd_p^{\delta} \quad (2)$$

where dN is the number of particles per unit water volume in the size range d_p to $[d_p + d(d_p)]$ [*Mari and Kiørboe*, 1996]. The factor k is a constant that depends on the total number of particles per volume, and δ ($\delta < 0$) describes the spectral slope of the size distribution. The less negative is δ, the greater is the fraction of larger gels. Both δ and k were derived from regressions of $\log[dN/d(d_p)]$ versus $\log[d_p]$.

Effects of a treatment, such as pCO_2 perturbation, during a mesocosms study can be identified against temporal variability by calculating the deviation of each treatment from the overall mean of the mesocosms [*Endres et al.*, 2014; *Engel et al.*, 2013]. Here deviations of each treatment (j) for days ($i = -1, \ldots, 29$) are given by $y_{ij} = (x_{ij} - \bar{y}_i)$, with $\bar{y}_i = \frac{1}{3}\sum_{j}^{3}(x_j)_i$, and are reported as mean deviation (MD) of absolute values, or as total deviation (TD) of values normalized to $\bar{y}_i$. We considered every treatment as an independent data set of replicate samples. Statistical tests were performed with SigmaPlot package (Systat Software Inc.). Statistical significance was accepted for $p < 0.05$. Pearson correlation coefficients and Spearman correlation coefficients were determined for normal and nonnormal distributed data, respectively, on all parameters over time (Figure 1). Detailed correlations according to the different CO_2 treatments are given in Table 1. Statistical significance of a CO_2 effect was determined with Kolmogorov-Smirnov tests on nonnormalized daily anomalies given the data being normal distributed (Table 2). Average values are reported with ±1 standard deviation.

Wind data have been retrieved from the free service provided by the Norwegian Meteorological Institute (http://eklima.met.no/).

3. Results and Discussion

3.1. Temporal Development of Biogenic Properties

3.1.1. Autotrophic Community in the Water Column and SML

Two phytoplankton blooms were observed in the water column of the mesocosms, as derived from increases in chlorophyll *a* concentrations (Figure 1a). In all mesocosms, the first bloom occurred around day 3 and was mainly dominated by chlorophyta and diatoms [*Endres et al.*, 2014; J. R. Bermúdez et al., personal communication, 2012). On day 3, the average chlorophyll *a* concentrations were 3.24 ± 0.25 μg L^{-1} (control), 3.59 ± 0.37 μg L^{-1} (medium pCO_2), and 3.58 ± 0.22 μg L^{-1} (high pCO_2). The second bloom was induced by the addition of nutrients, with average chlorophyll *a* concentrations at day 19 of 4.14 ± 0.19 μg L^{-1} (control), 4.62 ± 0.04 μg L^{-1} (medium pCO_2), and 3.41 ± 0.40 μg L^{-1} (high pCO_2) (Figure 1a). The main species observed during the second bloom phase were diatoms, cryptophythes, chlorophytes, and haptophytes (J. R. Bermúdez et al., personal communication, 2012). Generally, chlorophyll *a* showed the highest concentrations in the high pCO_2 treatment during the first bloom phase, while after the addition of nutrients highest values were recorded in the medium treatment. This pattern was also observed in a previous study [*Schulz et al.*, 2013] and suggests that nutrient availability can modify the response of a plankton

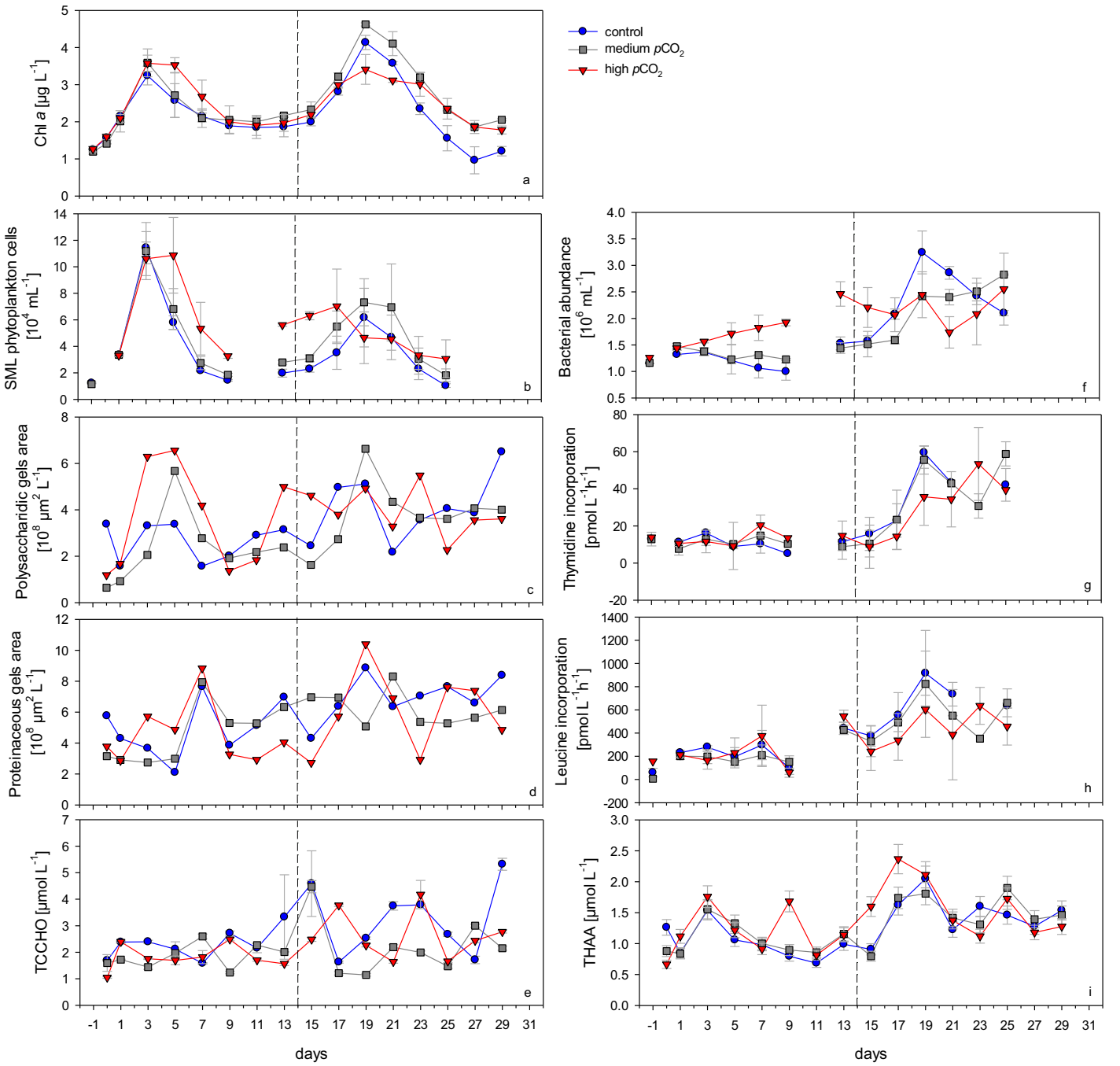

Figure 1. (a) Chlorophyll *a* concentrations measured in the water column and SML components per treatment: (b) phytoneuston abundance, (c) polysaccharidic marine gels area, (d) proteinaceous marine gels area, (e) total combined carbohydrates (TCCHO), (i) total hydrolyzable amino acids (THAA), (f) bacterial abundance and (g) activity as thymidine, and (h) leucine uptake rates. The CO_2 gradient was established on day 5, and on day 14 nutrients were added to the enclosed water in all mesocosms, as indicated by the black dashed line. The error bars in Figures 1a, 1b, 1f, 1g, and 1h are the standard deviations of the averaged values of two mesocosms as control (mesocosms 2 and 4), medium pCO_2 (mesocosms 1 and 8), and high pCO_2 (mesocosms 5 and 7). The error bars in Figures 1e and 1i refer to the analytical error. Error bars in Figures 1c and 1d are missing because the analysis was performed over one replicate (one filter) per treatment.

community to CO_2. In all treatments, phytoneuston abundance in the SML was significantly correlated to chlorophyll *a* concentration in the water column (Table 1), indicating a clear coupling of SML and bloom dynamics (Figure 1b). Over the whole experiment, the average abundance of phytoneuston was $3.6 \pm 2.9 \times 10^7$ cells mL^{-1} in control, $4.4 \pm 2.9 \times 10^7$ cells mL^{-1} in medium pCO_2, and $5.7 \pm 2.7 \times 10^7$ cells mL^{-1} at high pCO_2. In all treatments, highest phytoneuston abundances were observed around day 3 in

Table 1. Correlations Among Different Parameters Measured Within Each Treatment Based on Pearson Correlation Coefficient and Spearman Correlation Coefficient (*)[a]

Control	Phytoneuston Abundance	Polysaccharidic Gels	Proteinaceous Gels	TCCHO	THAA	Bacteria	Secondary Production (Thymidine)*	Secondary Production (Leucine)
Chl *a*	$p = 0.003$, $n = 14$					$p = 0.01$, $n = 13$		$p = 0.02$, $n = 12$
Phytoneuston abundance								
Polysaccharidic gels			$p = 0.048$, $n = 16$		$p < 0.001$, $n = 16$	$p = 0.046$, $n = 12$		$p = 0.045$, $n = 11$
Proteinaceous gels					$p = 0.025$, $n = 16$	$p = 0.024$, $n = 12$		$p = 0.006$, $n = 11$
TCCHO								
THAA						$p = 0.004$, $n = 12$	$p = 0.003$, $n = 11$	$p = 0.007$, $n = 11$
Bacterial abundance							$p < 0.001$, $n = 12$	$p < 0.001$, $n = 12$
Secondary production (Thymidine)*								$p < 0.001$, $n = 12$

Medium pCO_2	Phytoneuston Abundance	Polysaccharidic Gels	Proteinaceous Gels	TCCHO*	THAA	Bacterial Abundance*	Secondary Production (Thymidine)*	Secondary Production (Leucine)
Chl *a*	$p < 0.001$, $n = 14$	$p = 0.01$, $n = 16$			$p = 0.01$, $n = 16$	$p = 0.04$, $n = 13$	$p = 0.03$, $n = 13$	$p = 0.01$, $n = 13$
Phytoneuston abundance								
Polysaccharidic gels					$p = 0.005$, $n = 16$		$p = 0.028$, $n = 12$	
Proteinaceous gels								
TCCHO*								
THAA							$p = 0.006$, $n = 12$	$p = 0.010$, $n = 12$
Bacterial abundance*							$p = 0.009$, $n = 13$	$p < 0.001$, $n = 13$
Secondary production (Thymidine)*								$p = 0.010$, $n = 13$

High pCO_2	Phytoneuston Abundance	Polysaccharidic Gels	Proteinaceous Gels	TCCHO*	THAA	Bacterial Abundance	Secondary Production (Thymidine)*	Secondary Production (Leucine)
Chl a	$p = 0.018$, $n = 13$	$p = 0.002$, $n = 16$						
Phytoneuston abundance		$p = 0.004$, $n = 13$						
Polysaccharidic gels								
Proteinaceous gels								
TCCHO*								
THAA								
Bacterial abundance								$p = 0.011$, $n = 13$
Secondary production (Thymidine)*								$p = 0.001$, $n = 13$

[a]Only values for $p < 0.05$ or $p = 0.05$ are shown.

concomitance with the first phytoplankton bloom in the underlying water yielding $11.4 \pm 1.2 \times 10^7$ cells mL^{-1} (control), $11.2 \pm 2.2 \times 10^7$ cells mL^{-1} (medium pCO_2), and $10.6 \pm 1.3 \times 10^7$ cells mL^{-1} (high pCO_2). After nutrient addition, highest phytoneuston abundances coincided with the second phytoplankton bloom peak around day 19, but, with generally lower values of $6.2 \pm 2.2 \times 10^7$ cells mL^{-1} (control), $7.3 \pm 1.8 \times 10^7$ cells mL^{-1} (medium pCO_2), and $4.6 \pm 1.9 \times 10^7$ cells mL^{-1} (high pCO_2).

Bloom development in the underlying water also influenced the organic composition of the SML. With increasing pCO_2, abundance of polysaccharidic gels in the SML became significantly related to chlorophyll *a*

AGU Journal of Geophysical Research: Oceans

10.1002/2014JC010188

Table 2. Deviations of Each Treatment From the Average Development of All Mesocosms Calculated for the Whole Experimental Period (t_{0-29}, t_{-1-25} for Bacterial Abundance and Activity) and From Day 0 to Day 15 (t_{0-15}, t_{-1-15} for Bacterial Abundance and Activity)[a]

	Proteinaceous Gels ($10^8 \mu m^2\ L^{-1}$)			Polysaccharidic Gels ($10^8 \mu m^2\ L^{-1}$)			Total Hydrolizable Amino Acids ($\mu M\ L^{-1}$)			Total Combined Carbohydrates ($\mu M\ L^{-1}$)		
	Control	Medium pCO_2	High pCO_2	Control	Medium pCO_2	High pCO_2	Control	Medium pCO_2	High pCO_2	Control	Medium pCO_2	High pCO_2
t_{0-29}	0.39 ± 0.97	−0.15 ± 1.28	−0.24 ± 1.40	−0.02 ± 1.02	−0.32 ± 0.85	0.33 ± 1.09	−0.06 ± 0.18	−0.03 ± 0.14	0.08 ± 0.24	0.43 ± 0.66	−0.31 ± 0.65	−0.11 ± 0.70
(*p*, *n* = *16*)		0.19	0.14		0.38	0.35		0.60	0.08		0.003	0.031
t_{0-15}	0.18 ± 0.93	0.16 ± 1.15	−0.34 ± 1.36	−0.20 ± 1.03	−0.60 ± 0.77	0.80 ± 1.10	−0.08 ± 0.18	−0.05 ± 0.14	0.13 ± 0.26	0.36 ± 0.42	−0.05 ± 0.51	−0.31 ± 0.51
(*p*, *n* = *9*)		0.97	0.35		0.37	0.06		0.73	0.07		0.08	<0.01
	Bacterial Abundance ($10^6\ mL^{-1}$)			Leucine Uptake ($10\ pmol\ L^{-1}\ h^{-1}$)			Thymidine Uptake ($pmol\ L^{-1}\ h^{-1}$)			Phytoneuston Abundance ($10^7\ mL^{-1}$)		
	Control	Medium pCO_2	High pCO_2	Control	Medium pCO_2	High pCO_2	Control	Medium pCO_2	High pCO_2	Control	Medium pCO_2	High pCO_2
t_{-1-25}	−0.05 ± 0.31	−0.08 ± 0.20	0.13 ± 0.35	4.66 ± 6.38	−0.21 ± 4.80	−4.09 ± 9.23	0.69 ± 4.14	1.63 ± 3.96	−2.26 ± 5.40	−0.82 ± 0.79	−0.03 ± 0.76	0.76 ± 1.46
(*p*, *n* = *13*)		0.75	0.18		0.04	0.01		0.57	0.14		0.02	<0.01
t_{-1-15}	−0.20 ± 0.13	−0.13 ± 0.14	0.33 ± 0.23	1.25 ± 3.40	−2.56 ± 4.26	1.31 ± 6.39	−0.28 ± 3.15	−0.77 ± 1.27	1.05 ± 2.81	−0.84 ± 0.89	−0.43 ± 0.42	1.11 ± 1.53
(*p*, *n* = *8*)		0.33	<0.001		0.07	1		0.69	0.38		0.44	<0.01

[a]Deviations are reported as mean absolute values (MD) ± SD. Significance level (*p*) is based on Kolmogorov-Smirnov tests between control and treatments on normal distributed data.

concentration of the water column (Table 1). Phytoplankton exudation represents a specific source of polysaccharidic gels such as TEP [*Passow*, 2002b]. Under high CO_2 levels, the release of polysaccharidic precursors by phytoplankton has been shown to increase [*Borchard and Engel*, 2012] leading to higher gel particle abundance [*Engel*, 2002]. While organic matter composition of the SML is controlled by a variety of processes, a stimulating effect of CO_2 on phytoplankton could be one factor leading to a tighter coupling between concentrations of polysaccharidic gels in the SML and chlorophyll *a* in the water column.

3.1.2. Organic Matter: Marine Gels, Carbohydrates, and Amino Acids

Over the whole experiment, polysaccharidic gels in the SML averaged $3.4 \pm 1.3 \times 10^8$ μm^2 L^{-1} (control), $3.1 \pm 1.6 \times 10^8$ μm^2 L^{-1} (medium pCO_2), and $3.7 \pm 1.7 \times 10^8$ μm^2 L^{-1} (high pCO_2). Polysaccharidic gels were generally less abundant than proteinaceous gels with $5.9 \pm 1.9 \times 10^8$ μm^2 L^{-1} (control), $5.4 \pm 1.7 \times 10^8$ μm^2 L^{-1} (medium pCO_2), and $5.3 \pm 2.4 \times 10^8$ μm^2 L^{-1} (high pCO_2). Whereas highest concentrations of polysaccharidic gels coincided with the first phytoplankton bloom peak (Figure 1c), abundance of proteinaceous particles was highest 4 days thereafter (Figure 1d). This delay in peak concentrations was not observed after nutrient addition, when proteinaceous gels as well as chlorophyll *a* concentrations were highest around day 19.

Bacterial degradation of organic compounds requires time and the presence of specific extracellular enzymes able to break up larger molecules for bacterial assimilation [*Arnosti*, 2011]. Extracellular enzymes released by marine bacteria as well as protein material derived from cell lysis can contribute to a biofilm matrix [*Flemming and Wingender*, 2010] and to proteinaceous gels [*Bar-Zeev et al*., 2012; *Long and Azam*, 1996]. We therefore suggest that extracellular proteins derived from bacterial decomposition of organic matter or extracellular enzymes themselves contributed to the built-up of the proteinaceous gel particles pool in the SML, thus explaining a delay of a couple of days. Bacterial abundances increased in the course of the experiment and were much higher during the second bloom. Thus, the impact of bacteria on the organic matter pool was likely more immediate at that time (Figure 1f).

After nutrient addition, total combined carbohydrates (TCCHO) in the SML reached higher values but were also more variable than during the first bloom period (Figure 1e). Average concentrations of TCCHO during the whole experiment were 2.8 ± 1.1 μmol L^{-1} (control), 2.0 ± 0.8 μmol L^{-1} (medium pCO_2), and 2.2 ± 0.8 μmol L^{-1} (high pCO_2). In contrast to polysaccharidic gels, TCCHO concentration was not significantly related to the chlorophyll *a* development in any treatment (Table 1).

Average total hydrolysable amino acids (THAA) concentrations during the whole experiment were 1.2 ± 0.4, 1.3 ± 0.4, and 1.4 ± 0.5 μmol L^{-1} in control, medium, and high pCO_2 treatments, respectively. In contrast to TCCHO, development of THAA concentration in the SML resembled more the chlorophyll *a* development of the water column, with highest concentrations reached around bloom peak days 3 and 19 (Figure 1i). During the first phytoplankton bloom, THAA concentration in control treatment was 1.5 ± 0.2 μmol L^{-1}, in medium pCO_2 was 1.6 ± 0.2 μmol L^{-1}, and in high was pCO_2 1.8 ± 0.2 μmol L^{-1} (day 3). During the second phytoplankton bloom, 2.0 ± 0.2 μmol L^{-1} was the concentration of THAA for control (day 19), 1.8 ± 0.2 μmol L^{-1} in medium pCO_2 (day 19), and 2.4 ± 0.2 μmol L^{-1} was found in high pCO_2 (day 17). Concentrations of THAA as well as of TCCHO during this study were in good accordance with previous observations of the SML in natural marine systems [*Kuznetsova et al*., 2005; *Wurl and Holmes*, 2008].

3.1.3. Heterotrophic Response to Changes in the Organic Matter

Bacterial abundance and activity (BP) within the SML increased considerably after nutrient addition, showing a clear peak on day 19 concomitant to the second phytoplankton bloom (Figures 1f–1h). Average abundances were $1.8 \pm 0.7 \times 10^6$ cells mL^{-1} (control), $1.7 \pm 0.6 \times 10^6$ cells mL^{-1} (medium pCO_2), and $1.9 \pm 0.4 \times 10^6$ cells mL^{-1} (high pCO_2) (Figure 1f). Concomitant with bacterial abundance, also BP increased after nutrient addition. Thymidine uptake rates ranged from 5.12 to 20 pmol L^{-1} h^{-1} during the first bloom phase, and from 14 to 62 pmol L^{-1} h^{-1} during the second one. Range of leucine uptake rates were 60–546 pmol L^{-1} h^{-1}, and 336–916 pmol L^{-1} h^{-1} for the first and second bloom phases, respectively (Figures 1g and 1h).

Bacterial abundance and BP were positively correlated to THAA concentrations in the control and medium pCO_2 (Table 1) suggesting a contribution of bacterial biomass to the amino acids pool. According to our estimates of bacterial C and N contents, both N_{bac} and C_{bac} significantly correlated to THAA-N and THAA-C ($p < 0.05$, $n = 12$). The average contributions of N_{bac} and C_{bac} to THAA-N and THAA-C were 11.3 ± 2.3 (%-N_{bac}) and 22.1 ± 4.6 (%-C_{bac}).

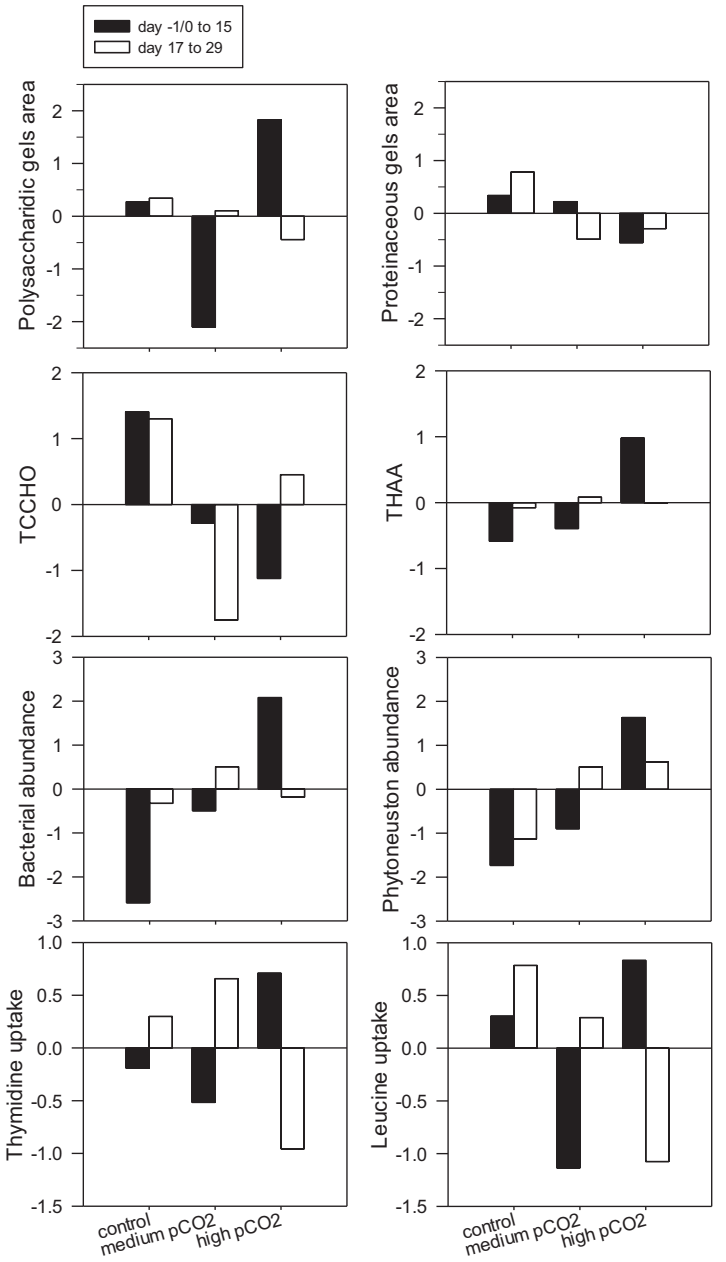

Figure 2. Effect of pCO_2 in the prenutrient addition phase (t_{0-15}, and t_{-1-15} for bacterial abundance and activity and phytoneuston abundance, black bars) and in the postnutrient addition phase (t_{17-29}, and t_{-1-25} for bacterial abundance and activity and phytoneuston abundance, white open bars).

3.1.4. The SML Reveals Strong Temporal Variability

Organic films at the sea-surface are suggested to affect the molecular diffusion of gases by inhibiting the transfer rates across the air-sea interface [*Liss and Duce*, 2005]. For this purpose, the thickness of the SML is a relevant parameter. In our mesocosms, we did not detect any significant differences of thickness between the treatments ($p = 0.442$). During the experiment the thickness of the SML increased slightly, yielding an average thickness of the SML in the prenutrient addition phase of $58 \pm 6 \times 10^{-4}$ and $69 \pm 5 \times 10^{-4}$ cm afterward. Average wind speeds were very similar in both phases, with 5.6 ± 2.4 m s^{-1} before nutrient addition and 5.7 ± 2.5 m s^{-1} thereafter. However, higher wind speeds were observed at certain days reaching 8.9 m s^{-1}, particularly during the second half of the experiment (day 17). Although it is not straightforward to establish a direct correlation between the wind speed and the thickness of the SML measured in enclosed bags as mesocosms, it has been previously shown that at higher wind speed the thickness of open sea SML collected can also be larger, depending on the wave state [*Carlson*, 1982; *Falkowska*, 1999]. Thus, some variability of SML parameters observed during the second half of the experiment may be due to increased turbulence inside the mesocosms.

3.2. Effect of pCO_2 on the SML Composition

Comparison of the three treatments revealed a potential effect of CO_2 on individual components of the SML, and a potential coeffect of nutrient availability. Therefore, we analyzed data for the whole experimental period, as well as for the period prior to nutrient addition separately (Table 2). Statistical significance levels are shown in Table 2. A pCO_2 impact on gel particles was not obvious. During the first bloom phase, total area of polysaccharidic gels was higher at high pCO_2 (Figure 1c), but differences between treatments were not significant, neither for the prebloom nor for the whole period (Table 2). Nutrient addition clearly coaffected

Table 3. Size Frequency Distribution Coefficients k and δ and Average Diameter (d_p, μm) for Marine Gel Particles From Day 0 to Day 15 in Each Treatment[a]

		Proteinaceous Gels			Polysaccharidic Gels		
$y = kx^{\delta}$		Control	Medium pCO_2	High pCO_2	Control	Medium pCO_2	High pCO_2
Average	k	20.1 ± 15.1	27.4 ± 14.4	36.6 ± 8.7*	75.7 ± 34.6	54.2 ± 29.5	87.6 ± 49.1
	δ	−1.50 ± 0.23	−1.63 ± 0.19	−1.77 ± 0.15*	−2.24 ± 0.15	−2.19 ± 0.11	−2.24 ± 0.18
Average d_p (μm)		2.0 ± 0.5	2.0 ± 0.4	1.5 ± 0.2*	1.2 ± 0.2	1.2 ± 0.3	1.2 ± 0.3

[a]The size distribution of marine gels followed the equation $y = kx^{\delta}$, with y (μL^{-1}) being the particles number per size class x (μm), and k (μL^{-1}), and δ as the spectral slope of the curve. After day 15, combined effects of nutrient addition and CO_2 are difficult to discern. Stars (*) indicate statistically significant differences determined with Kolmogorov-Smirnov tests run on nonnormalized anomalies over the daily average value of all mesocosms until day 15 (* = different from control, $p < 0.05$).

polysaccharidic gel abundance in the SML (Figure 2). During the first bloom phase, polysaccharidic gel particles showed a strong positive anomaly, i.e., positive total deviation, in the high pCO_2 treatment. After nutrient addition, this pattern was reversed and even a slight negative anomaly was observed.

No significant effect of CO_2 on proteinaceous gel concentration was revealed either (Table 2). However, proteinaceous gel seemed to respond differently to the CO_2 treatment compared to polysaccharidic gels. There was a steep decrease in total area of proteinaceous gels in the wake of the bloom peaks, particularly pronounced at high compared to control and medium pCO_2 (Figure 1d). For both bloom phases, TD values observed at high pCO_2 for proteinaceous gels were negative, while positive in the control (Figure 2). Also THAA and TCCHO showed a rather opposite behavior with respect to a CO_2 response. THAA concentrations at high pCO_2 were generally higher than in the control treatment in both, the total experimental period and prenutrient addition phase, while TCCHO concentrations were significantly lower at higher pCO_2 levels (Table 2). Higher THAA concentrations at high pCO_2 might be related to higher bacterial biomass contributing to the amino acid pool as bacteria were estimated being up to ∼22% of THAA-Carbon. Lower TCCHO concentration at high pCO_2 especially in the prenutrient addition phase could reflect the higher bacterial abundance and enhanced heterotrophic degradation activity [*Piontek et al*., 2010] but may also be related to an enhanced formation of polysaccharidic gels within the SML [*Engel et al*., 2004; *Wurl et al*., 2011a]. Like for proteinaceous gels, nutrient addition did not seem to change the response of THAA to the CO_2 treatment (Figure 2).

Up to day 17, phytoneuston abundance was higher at high pCO_2 (Figure 1b), and the analysis of daily anomalies revealed a positive effect of CO_2 on phytoneuston abundances in both prenutrient addition and postnutrient addition phases (Figure 2 and Table 2). Bacterial abundances in the SML were higher at high pCO_2 before nutrient addition and significantly different to the control (Figure 2 and Table 2). This observation agrees well with earlier findings of increased bacterial abundance at high CO_2 in the water column of previous mesocosm experiments [*Engel et al*., 2014; *Grossart et al*., 2006] and of the present experiment [*Endres et al*., 2014]. After the addition of nutrients on day 14, higher bacterial abundances in the SML were observed in the control and medium CO_2 mesocosms (Figures 1f and 2). This decrease of bacterial abundances at high pCO_2 during the later phase of the experiment may be related to the observed decrease of polysaccharidic gels, being a substrate of bacteria to attach and grow upon. Despite the stimulating effect of high pCO_2 on bacterial abundance during the first bloom phase, BP was not enhanced (Figure 2 and Table 2). After nutrient addition, BP rather decreased with increasing CO_2, yielding overall lower rates in the high pCO_2 treatment compared to the control, as revealed from Leucine uptake (Figure 2 and Table 2). It has been suggested that ascending polysaccharidic gels may act as a vehicle for bacterial transport from the water column to the SML [*Azetsu and Passow*, 2004]. Thus, an increment in polysaccharidic gels during the first bloom phase could be one factor for increasing bacterial abundance in the SML of high pCO_2. A passive transport of gel particles and bacteria to the SML may also explain the observed differences between bacterial abundance and activity (BP).

In the first bloom phase, as bacterial abundance in the SML benefited from increasing pCO_2, proteinaceous gels were found in lower concentrations (Figure 2). This observation corroborates previous findings of high rates of extracellular peptide hydrolysis [*Kuznetsova and Lee*, 2001], and high bacterial uptake rates of amino acids [*Donderski et al*., 1998] in the SML, suggesting a preferential degradation of proteins as valuable nutritional substrate. Thus bacteria thriving under high pCO_2 could be responsible for a decrease of proteinaceous

Table 4. Average Abundance (μL^{-1}, Day 0–Day 15) of Marine Gels in the SML for Different pCO_2 Levels and the Relative Contribution (%) of Two Different Size Classes (μm) to Total Gel Abundance

	Control		Medium pCO_2		High pCO_2	
μm	μL^{-1}	%	μL^{-1}	%	μL^{-1}	%
Proteinaceous Gels—Total Period						
0.4–1	18.7 ± 23.7	43.3 ± 24.1	17.3 ± 8.3	46.7 ± 15.4	32.5 ± 15.8	55.5 ± 13.4
>1	16.4 ± 8.2	56.7 ± 24.1	20.3 ± 8.2	53.3 ± 15.4	23.5 ± 8.8	44.5 ± 13.4
Polysaccharidic Gels—Total Period						
0.4–1	61.9 ± 40.1	63.2 ± 7.1	39.2 ± 19.0	59.8 ± 4.9	56.0 ± 29.0	59.0 ± 5.4
>1	31.0 ± 9.6	36.8 ± 7.1	25.6 ± 13.7	40.2 ± 4.9	37.2 ± 18.0	41.0 ± 5.4

gels area by means of degradation activity, which is ultimately reflected in more but smaller gel particles (Table 3). A previous mesocosm study proposed that higher heterotrophic activity might counteract CO_2 fixation by autotrophs [*Engel et al*., 2013] providing oceanic sources of CO_2 to the atmosphere [*Del Giorgio and Duarte*, 2002]. This might be particularly relevant for the SML too, as enhanced heterotrophic processes may result in higher pCO_2 at the very surface of the ocean. Hence, bacterial activity associated to the presence of marine gels might influence the role of the SML in mediating air-sea gas exchange [*Cunliffe et al*., 2013].

3.3. Marine Gel Size-Distribution Within the SML

The abundance and size of marine gels in subsurface waters and in the SML determine their potential fate as CCN in the atmosphere [*Orellana et al*., 2011]. pH is known to alter size of gels by promoting a volume phase transition [*Chin et al*., 1998; *Orellana et al*., 2011] and may affect the dynamics of nascent POA. In order to identify a potential effect of the CO_2 manipulation on gel size, we analyzed the size-frequency distribution of polysaccharidic and proteinaceous gels in all treatments from day 0 to day 15, i.e., during the first bloom phase (Tables 3 and 4, Figure 3) according to equation (2) as described in section 2. In general, proteinaceous gels were larger but less abundant compared to polysaccharidic ones (Tables 3 and 4, Figure 3). However, high pCO_2 promoted a significant increase in abundance (Table 3, $p < 0.05$, $n = 9$) and a significant decrease in size, d_p, of proteinaceous gels (Table 3, $p < 0.01$, $n = 9$). This again could be partly explained by increasing bacterial degradation of proteinaceous compounds in the SML under more acidic conditions. For proteinaceous gels, the contribution of the smallest size fraction (0.4–1 μm) to the total abundance increased along with rising CO_2 levels (Table 4). For polysaccharidic gels instead, particles smaller than 1 μm always contributed most to total gel abundance in the SML, up to 63.2% (Table 4), in accordance with the assumption of gels being formed by assembly of smaller precursors [*Chin et al*., 1998].

During biologically productive periods, marine POA reveal a high fraction of water insoluble organic particles [*O'Dowd et al*., 2004], of polysaccharidic gel-like composition [*Orellana et al*., 2011; *Russell et al*., 2010]. In the ocean, high abundance of polysaccharidic gels has been related to phytoplankton blooms [*Mari and Kiørboe*, 1996; *Passow*, 2002b]. According to our study, polysaccharidic gels in the SML were tightly coupled to phytoplankton dynamics especially at high pCO_2. For both classes of marine gels that we investigated, their dynamics in the SML and in future ocean scenarios were closely related to autotrophic and heterotrophic metabolism. Proteinaceous gels contributed even more to the SML gel-like composition, and may explain the enrichment of proteinaceous material in natural SML samples and in sea-spray aerosols [*Kuznetsova et al*., 2005]. High surface-active properties of amino acids in addition to the active bacterial release of DOM as extracellular enzymes or by cell lysis contribute to a biofilm matrix [*Flemming and Wingender*, 2010] and may support proteinaceous gel accumulation at present CO_2 levels (control treatment) as observed during this study. Following our results, acidification of seawater has a high potential to affect the amount and composition of organic matter, in particular with respect to gel particles, in the SML. Organic matter in the SML thus reflects the sensitivity of marine microorganisms in the surface ocean to environmental change, which was shown during previous mesocosms studies [*Engel et al*., 2013; *Riebesell et al*., 2009; *Schulz et al*., 2013]. Altered characteristics of the SML could be relevant for air-sea gas exchange, when affecting capillary wave damping and molecular diffusion of gases [*Liss and Duce*, 2005]. Size and chemical mixing state of particles, that is, the way chemical components are mixed at the level of a single particle, are two essential factors that determine particles' interaction with the climate system such as hygroscopicity and their ability to scatter radiation or act as CCN [*Bauer et al*.,

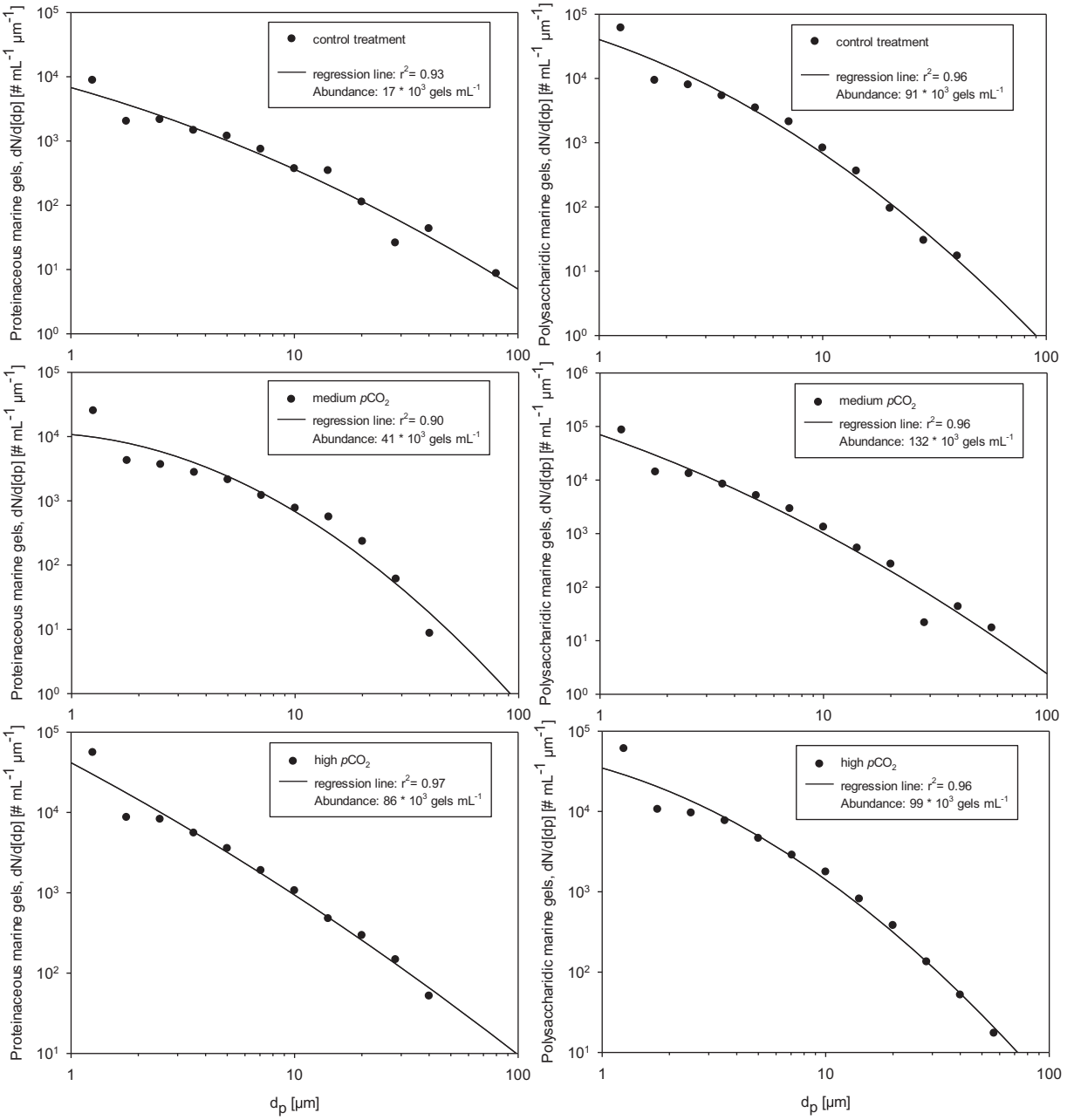

Figure 3. Logarithmic distribution of the size frequency spectra and abundance of (left) proteinaceous and (right) polysaccharidic marine gel particles according to the different pCO_2 treatments on day 5, when the CO_2 addition was finalized. The regression line is based on a power law relationship according to equation (2) as described in section 2.

2013; *Collins et al*., 2013; *Prather et al*., 2013]. Organic compounds in aerosols can reduce the surface tension of droplets facilitating the CCN potential and growth [*Andreae and Rosenfeld*, 2008]. The presence of an active SML bacterial community mediating marine gels dynamics and DOM turnover might influence the composition and the CCN activation potential of nascent marine aerosols [*Collins et al*., 2013; *Prather et al*., 2013]. Atmospheric CCN density and concentrations of greenhouse gases control the earth's radiative budget [*Solomon et al*., 2007]. These two main driving forces may be tightly connected to the properties of the marine air-water interface and subsurface waters.

We suggest that the coupling between SML organic components and microbial communities makes the top millimeter of the ocean a climate-sensitive environment. An improved understanding of its

Acknowledgments
We would like to thank all participants of the Bergen Mesocosms study, in particular U. Riebesell, J. Czerny, A. Ludwig, M. Meyerhofer, and the KOSMOS team for mesocosms implementation and logistics, as well as the staff of the Marine Biological Station of Bergen University for hosting the experiment and technical support. We thank the captains and crews of R/V Håkon Mosby, R/V Alkor, and R/V Heincke for support during transport, deployment, and recovery of the mesocosm facility. Big, special thanks go to the sampling team: L. Bach, M. Sswatt, and T. Lipsewers. S. Koch-Klavsen is gratefully acknowledged for measuring chlorophyll concentrations, J. R. Bermúdez for phytoplankton characterization in the water column, R. Flerus and J. Roa for amino acids and carbohydrates analysis, respectively. Helpful comments and stimulating discussions with C. Borchard and J. Piontek are also greatly appreciated. Moreover, M. Schartau is greatly acknowledged for friendly review and suggestions for data analysis. This work was supported by BMBF project SOPRAN II (Surface Ocean Processes in the Anthropocene, 03F0611C-TP01 and 03F0611B-TP02) and BIOACID (03F0608B), and is a contribution to the international SOLAS program. All data presented in this manuscript are available upon request and will be submitted to the PANGAEA database (http://www.pangaea.de).

structure and dynamics will help to better estimate ocean-atmosphere interactions in a future high CO_2 world.

References

Andreae, M. O., and D. Rosenfeld (2008), Aerosol-cloud-precipitation interactions. Part 1. The nature and sources of cloud-active aerosols, *Earth Sci. Rev.*, *89*(Part 1), 13–41, doi:10.1016/j.earscirev.2008.03.001.

Arnosti, C. (2011), Microbial extracellular enzymes and the marine carbon cycle, *Annu. Rev. Mar. Sci.*, *3*(1), 401–425, doi:10.1146/annurev-marine-120709-142731.

Azetsu, S. K., and U. Passow (2004), Ascending marine particles: Significance of transparent exopolymer particles (TEP) in the upper ocean, *Limnol. Oceanogr. Methods*, *49*, 741–748, doi:10.4319/lo.2004.49.3.0741.

Bar-Zeev, E., I. Berman-Frank, O. Girshevitz, and T. Berman (2012), Revised paradigm of aquatic biofilm formation facilitated by microgel transparent exopolymer particles, *Proc. Natl. Acad. Sci. U. S. A.*, *109*(23), 9119–9124, doi:10.1073/pnas.1203708109.

Bauer, S. E., A. Ault, and K. A. Prather (2013), Evaluation of aerosol mixing state classes in the GISS modelE-MATRIX climate model using single-particle mass spectrometry measurements, *J. Geophys. Res. Atmos.*, *118*, 9834–9844, doi:10.1002/jgrd.50700.

Borchard, C., and A. Engel (2012), Organic matter exudation by *Emiliania huxleyi* under simulated future ocean conditions, *Biogeosciences*, *9*(8), 3405–3423, doi:10.5194/bg-9-3405-2012.

Caldeira, K., and M. E. Wickett (2003), Oceanography: Anthropogenic carbon and ocean pH, *Nature*, *425*(6956), 365–365, doi:10.1038/425365a.

Carlson, D. J. (1982), A field evaluation of plate and screen microlayer sampling techniques, *Mar. Chem.*, *11*, 189–208, doi:10.1016/0304-4203(82)90015-9.

Chin, W.-C., M. V. Orellana, and P. Verdugo (1998), Spontaneous assembly of marine dissolved organic matter into polymer gels, *Nature*, *391*(6667), 568–572, doi:10.1038/35345.

Chin-Leo, G., and D. L. Kirchman (1988), Estimating bacterial production in marine waters from the simultaneous incorporation of thymidine and leucine, *Appl. Environ. Microbiol.*, *54*, 1934–1939.

Collins, D. B., et al. (2013), Impact of marine biogeochemistry on the chemical mixing state and cloud forming ability of nascent sea spray aerosol, *J. Geophys. Res. Atmos.*, *118*, 8553–8565, doi:10.1002/jgrd.50598.

Cunliffe, M., and J. C. Murrell (2009), The sea-surface microlayer is a gelatinous biofilm, *ISME J.*, *3*(9), 1001–1003, doi:10.1038/ismej.2009.69.

Cunliffe, M., R. C. Upstill-Goddard, and J. C. Murrell (2011), Microbiology of aquatic surface microlayers, *FEMS Microbiol. Rev.*, *35*(2), 233–246, doi:10.1111/j.1574-6976.2010.00246.x.

Cunliffe, M., A. Engel, S. Frka, B. Gašparović, C. Guitart, J. C. Murrell, M. Salter, C. Stolle, R. Upstill-Goddard, and O. Wurl (2013), Sea surface microlayers: A unified physicochemical and biological perspective of the air-ocean interface, *Prog. Oceanogr.*, *109*, 104–116, doi:10.1016/j.pocean.2012.08.004.

Del Giorgio, P. A., and C. M. Duarte (2002), Respiration in the open ocean, *Nature*, *420*(6914), 379–384, doi:10.1038/nature01165.

Donderski, W., Z. Mudryk, and M. Walczak (1998), Utilization of low molecular weight organic compounds by marine neustonic and planktonic bacteria, *Pol. J. Environ. Stud.*, *7*(5), 279–283.

Endres, S., L. Galgani, U. Riebesell, K. G. Schulz, and A. Engel (2014), Stimulated bacterial growth under elevated pCO_2: Results from an offshore mesocosm study, *PLoS One*, *9*(7), e103694, doi:10.1371/journal.pone.0103694.

Engel, A. (2002), Direct relationship between CO_2 uptake and transparent exopolymer particles production in natural phytoplankton, *J. Plankton Res.*, *24*(1), 49–53, doi:10.1093/plankt/24.1.49.

Engel, A. (2009), Determination of marine gel particles, in *Practical Guidelines for the Analysis of Seawater*, edited by O. Wurl, pp. 125–142, CRC Press, Boca Raton, Fla.

Engel, A., and N. Händel (2011), A novel protocol for determining the concentration and composition of sugars in particulate and in high molecular weight dissolved organic matter (HMW-DOM) in seawater, *Mar. Chem.*, *127*(1–4), 180–191, doi:10.1016/j.marchem.2011.09.004.

Engel, A., S. Thoms, U. Riebesell, E. Rochelle-Newall, and I. Zondervan (2004), Polysaccharide aggregation as a potential sink of marine dissolved organic carbon, *Nature*, *428*(6986), 929–932, doi:10.1038/nature02453.

Engel, A., C. Borchard, J. Piontek, K. G. Schulz, U. Riebesell, and R. Bellerby (2013), CO_2 increases ^{14}C primary production in an Arctic plankton community, *Biogeosciences*, *10*(3), 1291–1308, doi:10.5194/bg-10-1291-2013.

Engel, A., J. Piontek, H. P. Grossart, U. Riebesell, K. G. Schulz, and M. Sperling (2014), Impact of CO_2 enrichment on organic matter dynamics during nutrient induced coastal phytoplankton blooms, *J. Plankton Res.*, *36*(3), 641–657, doi:10.1093/plankt/fbt125.

Fagerbakke, K. M., M. Heldal, and S. Norland (1996), Content of carbon, nitrogen, oxygen, sulfur and phosphorus in native aquatic and cultured bacteria, *Aquat. Microb. Ecol.*, *10*(1), 15–27, doi:10.3354/ame010015.

Falkowska, L. (1999), Sea surface microlayer: A field evaluation of teflon plate, glass plate and screen sampling techniques. Part 1. Thickness of microlayer samples and relation to wind speed, *Oceanologia*, *41*(2), 211–221.

Flemming, H.-C., and J. Wingender (2010), The biofilm matrix, *Nat. Rev. Microbiol.*, *8*(9), 623–633, doi:10.1038/nrmicro2415.

Grossart, H. P., M. Allgaier, U. Passow, and U. Riebesell (2006), Testing the effect of CO_2 concentration on the dynamics of marine heterotrophic bacterioplankton, *Limnol. Oceanogr. Methods*, *51*(1), 1–11, doi:10.4319/lo.2006.51.1.0001.

Harvey, G. W., and L. A. Burzell (1972), A simple microlayer method for small samples, *Limnol. Oceanogr.*, *11*, 608–614.

Hein, M., and K. Sand-Jensen (1997), CO_2 increases oceanic primary production, *Nature*, *388*(6642), 526–527.

Kuznetsova, M., and C. Lee (2001), Enhanced extracellular enzymatic peptide hydrolysis in the sea-surface microlayer, *Mar. Chem.*, *73*(3–4), 319–332, doi:10.1016/S0304-4203(00)00116-X.

Kuznetsova, M., C. Lee, and J. Aller (2005), Characterization of the proteinaceous matter in marine aerosols, *Mar. Chem.*, *96*(3–4), 359–377, doi:10.1016/j.marchem.2005.03.007.

Lechtenfeld, O. J., B. P. Koch, B. Gašparović, S. Frka, M. Witt, and G. Kattner (2013), The influence of salinity on the molecular and optical properties of surface microlayers in a karstic estuary, *Mar. Chem.*, *150*(0), 25–38, doi:10.1016/j.marchem.2013.01.006.

Leck, C., and E. K. Bigg (2005), Source and evolution of the marine aerosol—A new perspective, *Geophys. Res. Lett.*, *32*, L19803, doi:10.1029/2005GL023651.

Lindroth, P., and K. Mopper (1979), High performance liquid chromatographic determination of subpicomole amounts of amino acids by precolumn fluorescence derivatization with o-phthaldialdehyde, *Anal. Chem.*, *51*(11), 1667–1674, doi:10.1021/ac50047a019.

Liss, P. S., and R. A. Duce (2005), *The Sea Surface and Global Change*, Cambridge Univ. Press, Cambridge, U. K.

Long, R. A., and F. Azam (1996), Abundant protein-containing particles in the sea, *Aquat. Microb. Ecol.*, *10*(3), 213–221, doi:10.3354/ame010213.

Mari, X., and T. Kiørboe (1996), Abundance, size distribution and bacterial colonization of transparent exopolymeric particles (TEP) during spring in the Kattegat, *J. Plankton Res.*, *18*(6), 969–986, doi:10.1093/plankt/18.6.969.

Marie, D., X. L. Shi, F. Rigaut-Jalabert, and D. Vaulot (2010), Use of flow cytometric sorting to better assess the diversity of small photosynthetic eukaryotes in the English Channel, *FEMS Microbiol. Ecol.*, *72*(2), 165–178, doi:10.1111/j.1574-6941.2010.00842.x.

O'Dowd, C. D., M. C. Facchini, F. Cavalli, D. Ceburnis, M. Mircea, S. Decesari, S. Fuzzi, Y. J. Yoon, and J.-P. Putaud (2004), Biogenically driven organic contribution to marine aerosol, *Nature*, *431*(7009), 676–680, doi:10.1038/nature02959.

Orellana, M. V., P. A. Matrai, C. Leck, C. D. Rauschenberg, A. M. Lee, and E. Coz (2011), Marine microgels as a source of cloud condensation nuclei in the high Arctic, *Proc. Natl. Acad. Sci. U. S. A.*, *108*(33), 13,612–13,617, doi:10.1073/pnas.1102457108.

Passow, U. (2002b), Transparent exopolymer particles (TEP) in aquatic environments, *Prog. Oceanogr.*, *55*, 287–333, doi:10.1016/S0079-6611(02)00138-6.

Piontek, J., M. Lunau, N. Händel, C. Borchard, M. Wurst, and A. Engel (2010), Acidification increases microbial polysaccharide degradation in the ocean, *Biogeosciences*, *7*(5), 1615–1624, doi:10.5194/bg-7-1615-2010.

Prather, K. A., et al. (2013), Bringing the ocean into the laboratory to probe the chemical complexity of sea spray aerosol, *Proc. Natl. Acad. Sci. U. S. A.*, *110*(19), 7550–7555, doi:10.1073/pnas.1300262110.

Quinn, P. K., and T. S. Bates (2011), The case against climate regulation via oceanic phytoplankton sulphur emissions, *Nature*, *480*(7375), 51–56, doi:10.1038/nature10580.

Riebesell, U., A. Kortzinger, and A. Oschlies (2009), Sensitivities of marine carbon fluxes to ocean change, *Proc. Natl. Acad. Sci. U. S. A.*, *106*(49), 20,602–20,609, doi:10.1073/pnas.0813291106.

Riebesell, U., et al. (2013), Technical note: A mobile sea-going mesocosm system—New opportunities for ocean change research, *Biogeosciences*, *10*(3), 1835–1847, doi:10.5194/bg-10-1835-2013.

Russell, L. M., L. N. Hawkins, A. A. Frossard, P. K. Quinn, and T. S. Bates (2010), Carbohydrate-like composition of submicron atmospheric particles and their production from ocean bubble bursting, *Proc. Natl. Acad. Sci. U. S. A.*, *107*(15), 6652–6657, doi:10.1073/pnas.0908905107.

Sabine, C. L., et al. (2004), The oceanic sink for anthropogenic CO_2, *Science*, *305*(5682), 367–371, doi:10.1126/science.1097403.

Schulz, K. G., et al. (2013), Temporal biomass dynamics of an Arctic plankton bloom in response to increasing levels of atmospheric carbon dioxide, *Biogeosciences*, *10*(1), 161–180, doi:10.5194/bg-10-161-2013.

Solomon, S., D. Qin, M. Manning, Z. Chen, M. Marquis, K. B. Averyt, M. Tignor, and H. L. Miller (2007), *Climate Change 2007: The Physical Science Basis. Contribution of Working Group I to the Fourth Assessment Report of the Intergovernmental Panel on Climate Change*, Cambridge Univ. Press, Cambridge, U. K.

Verdugo, P. (2012), Marine microgels, *Annu. Rev. Mar. Sci.*, *4*(1), 375–400, doi:10.1146/annurev-marine-120709-142759.

Verdugo, P., A. L. Alldredge, F. Azam, D. L. Kirchman, U. Passow, and P. H. Santschi (2004), The oceanic gel phase: A bridge in the DOM–POM continuum, *Mar. Chem.*, *92*(1–4), 67–85, doi:10.1016/j.marchem.2004.06.017.

Welschmeyer, N. A. (1994), Fluorometric analysis of chlorophyll a in the presence of chlorophyll b and pheopigments, *Limnol. Oceanogr.*, *39*(8), 1985–1992, doi:10.4319/lo.1994.39.8.1985.

Wurl, O., and M. Holmes (2008), The gelatinous nature of the sea-surface microlayer, *Mar. Chem.*, *110*(1–2), 89–97, doi:10.1016/j.marchem.2008.02.009.

Wurl, O., L. Miller, and S. Vagle (2011a), Production and fate of transparent exopolymer particles in the ocean, *J. Geophys. Res.*, *116*, C00H13, doi:10.1029/2011JC007342.

Wurl, O., E. Wurl, L. Miller, K. Johnson, and S. Vagle (2011b), Formation and global distribution of sea-surface microlayers, *Biogeosciences*, *8*(1), 121–135, doi:10.5194/bg-8-121-2011.

Zhou, J., K. Mopper, and U. Passow (1998), The role of surface-active carbohydrates in the formation of transparent exopolymer particles by bubble adsorption of seawater, *Limnol. Oceanogr.*, *43*, 1860–1871, doi:10.4319/lo.1998.43.8.1860.